NASA Technical Paper 3646

ARL–TR–923

Measurements of Heat Transfer, Flow, and Pressures in a Simulated Turbine Blade Internal Cooling Passage

Louis M. Russell
Lewis Research Center, Cleveland, Ohio

Douglas R. Thurman
U.S. Army Research Laboratory, Lewis Research Center, Cleveland, Ohio

Philip E. Poinsatte and Steven A. Hippensteele
Lewis Research Center, Cleveland, Ohio

December 1997

The NASA STI Program Office ... in Profile

Since its founding, NASA has been dedicated to the advancement of aeronautics and space science. The NASA Scientific and Technical Information (STI) Program Office plays a key part in helping NASA maintain this important role.

The NASA STI Program Office is operated by Langley Research Center, the lead center for NASA's scientific and technical information. The NASA STI Program Office provides access to the NASA STI Database, the largest collection of aeronautical and space science STI in the world. The Program Office is also NASA's institutional mechanism for disseminating the results of its research and development activities. These results are published by NASA in the NASA STI Report Series, which includes the following report types:

- TECHNICAL PUBLICATION. Reports of completed research or a major significant phase of research that present the results of NASA programs and include extensive data or theoretical analysis. Includes compilations of significant scientific and technical data and information deemed to be of continuing reference value. NASA counter-part of peer reviewed formal professional papers, but having less stringent limitations on manuscript length and extent of graphic presentations.

- TECHNICAL MEMORANDUM. Scientific and technical findings that are preliminary or of specialized interest, e.g., quick release reports, working papers, and bibliographies that contain minimal annotation. Does not contain extensive analysis.

- CONTRACTOR REPORT. Scientific and technical findings by NASA-sponsored contractors and grantees.

- CONFERENCE PUBLICATION. Collected papers from scientific and technical conferences, symposia, seminars, or other meetings sponsored or co-sponsored by NASA.

- SPECIAL PUBLICATION. Scientific, technical, or historical information from NASA programs, projects, and missions, often concerned with subjects having substantial public interest.

- TECHNICAL TRANSLATION. English-language translations of foreign scientific and technical material pertinent to NASA's mission.

Specialized services that help round out the STI Program Office's diverse offerings include creating custom thesauri, building customized databases, organizing and publishing research results ... even providing videos.

For more information about the NASA STI Program Office, you can:

- Access the NASA STI Program Home Page at http://www.sti.nasa.gov/STI-homepage.html

- E-mail your question via the Internet to help@sti.nasa.gov

- Fax your question to the NASA Access Help Desk at (301) 621-0134

- Phone the NASA Access Help Desk at (301) 621-0390

- Write to:
  NASA Access Help Desk
  NASA Center for AeroSpace Information
  800 Elkridge Landing Road
  Linthicum Heights, MD 21090-2934

Acknowledgments

The authors wish to express their appreciation to William Camperchioli of the Aeropropulsion Facilities and Experiments Division at the NASA Lewis Research Center and James Little of NYMA Corporation for guidance and assistance in the use of the automated pressure recording system. The authors also express their appreciation for the guidance and assistance provided by Timothy Bencic of the Aeropropulsion Facilities and Experiments Division, who pioneered the use of the pressure sensitive paint method at Lewis Research Center.

Available from

NASA Center for Aerospace Information
800 Elkridge Landing Road
Linthicum Heights, MD 21090-2934
Price Code: A03

National Technical Information Service
5287 Port Royal Road
Springfield, VA 22100
Price Code: A03

Measurements of Heat Transfer, Flow, and Pressures in a Simulated Turbine Blade Internal Cooling Passage

Louis M. Russell*
National Aeronautics and Space Administration
Lewis Research Center
Cleveland, Ohio 44135

Douglas R. Thurman
U.S. Army Research Center
Lewis Research Center
Cleveland, Ohio 44135

Philip E. Poinsatte and Steven A. Hippensteele
National Aeronautics and Space Administration
Lewis Research Center
Cleveland, Ohio 44135

Summary

An experimental study was made to obtain quantitative information on heat transfer, flow, and pressure distribution in a branched duct test section that had several significant features of an internal cooling passage of a turbine blade. The objective of this study was to generate a set of experimental data that could be used for validation of computer codes that would be used to model internal cooling.

Surface heat transfer coefficients and entrance flow conditions were measured at nominal entrance Reynolds numbers of 45 000, 335 000, and 726 000. Heat transfer data were obtained by using a steady-state technique in which an Inconel heater sheet is attached to the surface and coated with liquid crystals. Visual and quantitative flow-field data from particle image velocimetry measurements for a plane at midchannel height for a Reynolds number of 45 000 were also obtained. The flow was seeded with polystyrene particles and illuminated by a laser light sheet. Pressure distribution measurements were made both on the surface with discrete holes and in the flow field with a total pressure probe. The flow-field measurements yielded flow-field velocities at selected locations. A relatively new method, pressure sensitive paint, was also used to measure surface pressure distribution. The pressure paint data obtained at Reynolds numbers of 335 000 and 726 000 compared well with the more standard method of measuring pressures by using discrete holes.

Introduction

A continuing objective in gas turbine technology is higher engine efficiency. One method of obtaining higher efficiency is the use of higher engine operating temperatures. Higher turbine inlet temperatures often require the use of internal cooling in the blades and vanes to maintain surface temperatures that the material can withstand for sustained periods of time. Thus, effective design of internal cooling passages is important and requires an understanding of the flow and temperature patterns. Good designs are also facilitated by the availability of dependable, validated computer codes, which are used to model the designs.

In recent years, there have been several attempts to numerically model internal flow and heat transfer by computer codes (refs. 1 and 2). Reference 1 points out that it is the combination of a complete experimental data base and accurate, efficient analytical tools that will ultimately shorten design times and optimize future turbines. Reference 3 further emphasizes the importance of coordination and cooperation between experimental and computational researchers in aeropropulsion systems. Reference 4 reports on a code prediction for a rotating square duct which was verified by experimental data.

For this report, an experimental study was performed to obtain quantitative visual information on flow and heat transfer in a test section which simulated the internal passage of a cooled radial turbine blade as described in reference 5. The objective of this study was to generate a set of experimental heat transfer, flow-field, and pressure data which could be used for validation of internal cooling computer codes.

Three nominal entrance Reynolds numbers, based on entrance hydraulic diameter, were investigated: 45 000, 335 000, and 726 000. Entrance velocity profiles and free-stream turbulence intensity were measured to establish upstream boundary conditions for computational purposes. Surface heat transfer coefficients were measured with a steady-state liquid crystal technique. Quantitative visual flow-field measurements by using particle

*Retired.

TABLE I.—AVAILABLE EXPERIMENTAL DATA
[Reynolds number based on entrance hydraulic diameter.]

Experimental data (technique used to obtain)	Reynolds number, Re		
	45 000	335 000	726 000
Midchannel velocity vectors (flow visualization)	X	----	----
Surface heat transfer on channel floor (liquid crystal)	X	X	X
Cross-section velocity vectors at 5 axial stations (5-hole probe) (ref. 7)	X	X	X
Surface static pressure (discrete pressure measurements)	X	X	X
Static pressures on channel floor (pressure sensitive paint)	----	X	X
Entrance free-stream turbulence intensities (hot-wire anemometry) (ref. 8)	X	X	X

image velocimetry were also obtained for a plane at midchannel height. Surface static pressure distributions from discrete hole measurements were determined as well as full flow-field total pressures, which yielded flow-field velocities that could be compared with the particle image velocimetry results. A relatively new method, pressure sensitive paint, was also used to measure surface pressure distribution. These results compared well with the results obtained by using discrete holes at Reynolds numbers of 335 000 and 726 000.

Computational results that used a commercially available code for the same configuration were reported in reference 6. This code was used to calculate flow-field velocities and surface heat transfer coefficients at Reynolds numbers matching some of the experimental results.

This report is intended to give the reader a brief summary of the results obtained. Not all of the results are presented; the reader is welcome to contact any of the authors for more information or to obtain additional data. Note also that limitations of some of the equipment prevented the acquisition of data at all three Reynolds numbers for each data set, that is, flow visualization data could only be obtained at Re = 45 000, and pressure paint data only at Re = 335 000 and 726 000. Table I shows the data available.

Nomenclature

A	heated area, m^2
D	hydraulic diameter, m
d	distance between interruptions in streaklines
E	voltage
h	heat transfer coefficient, $W/(m^2 - °K)$
P	pressure, N/m^2
Pr	Prandtl number
Q	heat rate, W
Re	Reynolds number based on entrance hydraulic diameter
r	recovery factor
T	temperature, °C
U_∞	free-stream velocity, m/sec
u	streamwise component of velocity
u^+	dimensionless velocity
v	horizontal component of velocity perpendicular to tunnel direction
w	vertical component of velocity perpendicular to tunnel direction
y	transverse distance, cm
y^+	dimensionless distance from floor
Q/A	heat flux
δ	boundary layer thickness, cm
ν	kinematic viscosity, m^2/sec
ρ	density, g/cm^3
τ_w	wall shear stress, N/m^2

Subscripts:

e	electrical heat input
entrance	test section entrance
L	loss
LC	liquid crystal
R	recovery
s	static
t	total
$theor$	theoretical

Apparatus

Figure 1 is a schematic of the overall test facility. Room temperature air was drawn through the tunnel by a vacuum exhaust system. The two-piece test section (fig. 2), was made of clear acrylic plastic and had a passage height of 5.08 cm. The width of the entrance section was 15.24 cm. The main test section was divided by a partition into two passages 12.7 cm wide, with the partition ending at the end of the test section. One passage was unobstructed and the other passage contained three rows of 0.95-cm-diameter pins in a staggered array. The pins were spaced 2.54 cm apart laterally, and the rows were spaced 2.54 cm apart. This configuration captures the significant features of the cooled radial turbine blade shown in figure 3 (from ref. 1), namely, the flow split created by a partition, the sharp corner, and cylindrical pins for turbulence generation. Entrance velocities were measured by using the differential between a wall static pressure tap and a total pressure probe at the entrance. Pressure, temperature, and flow data were recorded by commercial data acquisition systems. Photographic data were taken with one or more video cameras.

For the heat transfer tests, a 0.025-mm-thick Inconel sheet with a known uniform electrical resistance was attached to the floor of both the entrance and main test sections with a double coated adhesive material. Each Inconel sheet had copper bus bars spot-welded to it. The sheets were coated with black lacquer, then spray painted with thermochromic liquid crystals. A cross section of the test surface is shown in figure 4. A 2.5-cm-thick foam insulation prevented heat loss through the floor. For the heat transfer tests, the cylindrical pins were made of copper in order to simulate an actual blade where the surface heat is transferred to the pins. The unheated section of the tunnel upstream of the heated test surface was 60.96 cm long.

The test section for the flow visualization tests was identical in configuration to the heat transfer test section but without the liquid crystal-heater sheets and without the foam insulation. The pins for this model were made of clear acrylic plastic instead of copper. This allowed a laser light sheet to partially pass through the pins to illuminate the flow field.

The test section for the discrete hole pressure distribution tests was also identical in configuration to the heat transfer test section but with 57 pressure taps in the floor and the side walls at strategic locations. Both surface static pressures and flow field static and total pressures were measured at the locations shown in figure 5. The flow field was measured with a five-hole probe as shown in figure 6; the probe was constructed from five tubes of a 5.08-mm (0.02-in.) nominal diameter. In addition to total pressures, this probe was capable of determining direction of flow as well. All pressures were recorded with a computer-controlled, automated, electronic pressure recording system.

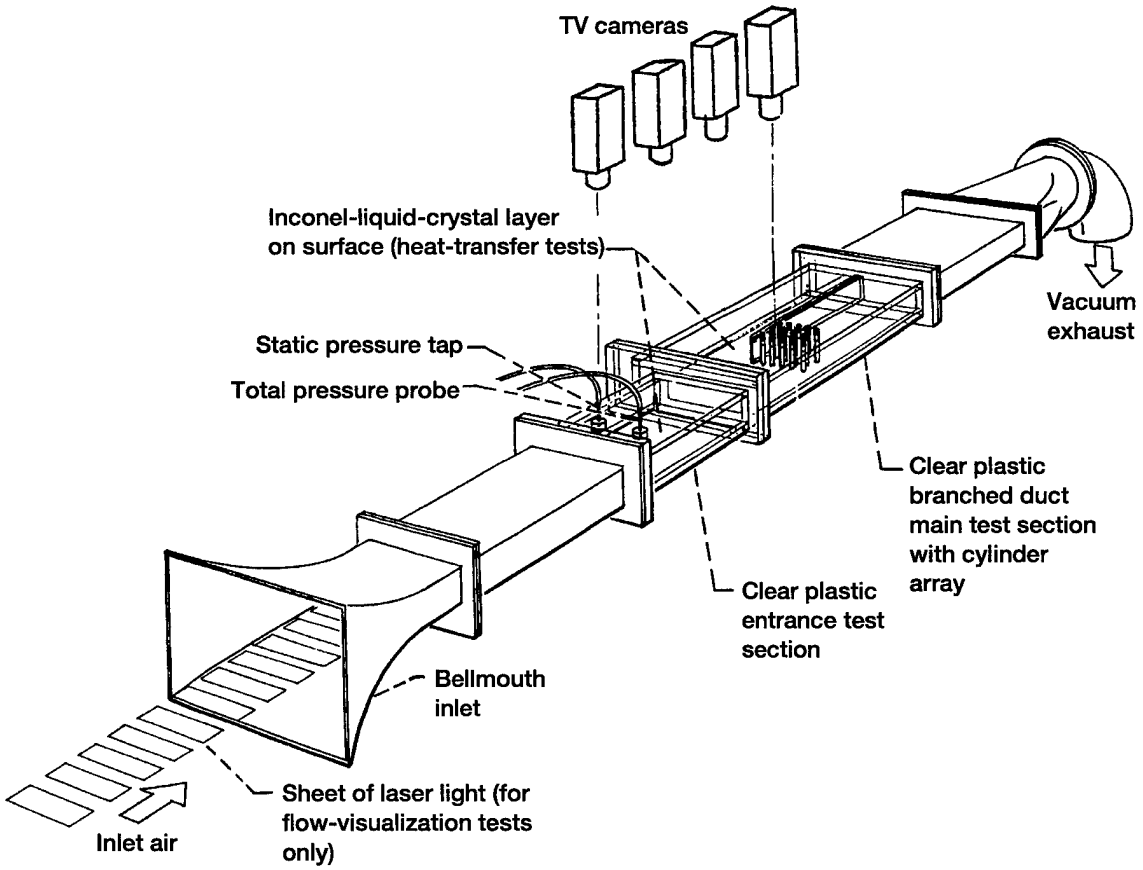

Figure 1.—Branched duct tunnel. (Only one camera used for flow-visualization tests.)

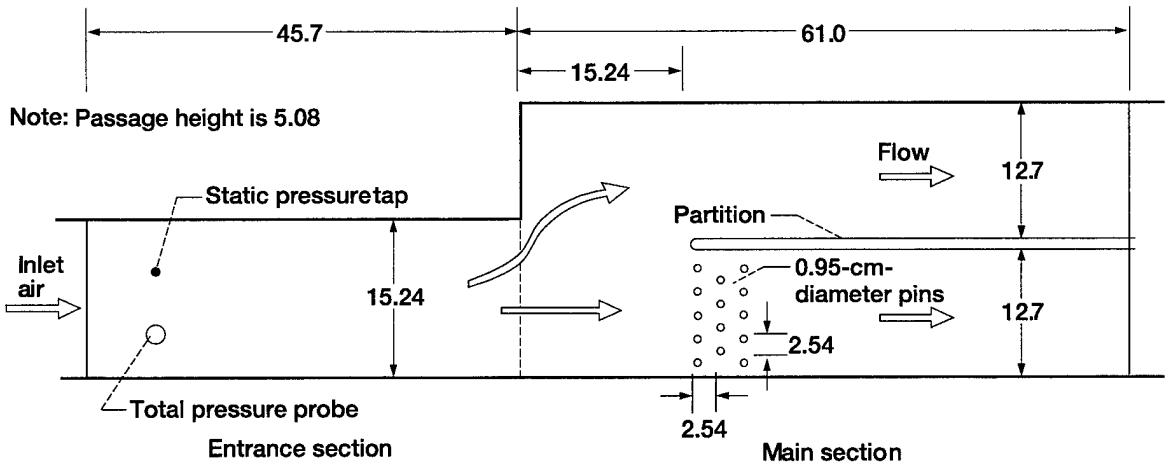

Figure 2.—Test section. (All dimensions given in centimeters.)

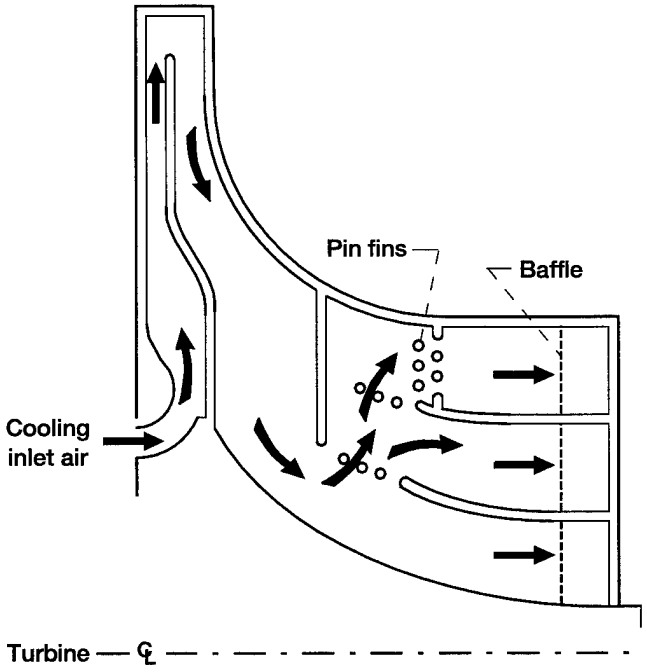

Figure 3.—Cooled radial turbine blade (ref. 1).

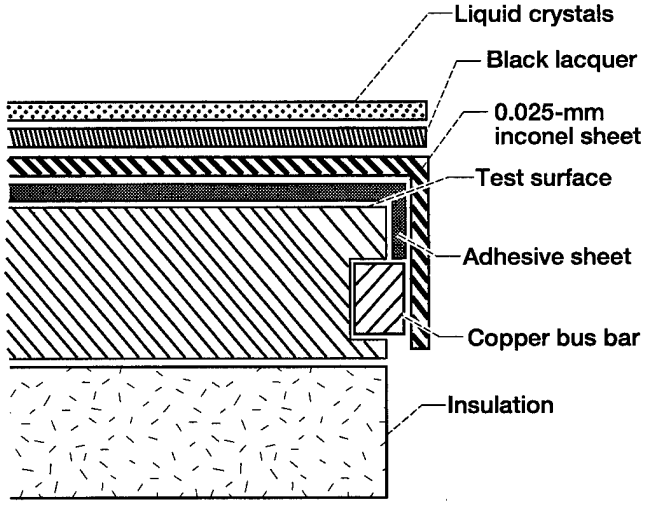

Figure 4.—Cross section of test surface.

Procedure

Liquid Crystal Calibration

Liquid crystals, by virtue of their property of changing color with temperature, provide a means of measuring surface temperature and visualizing thermal patterns at any desired location. The liquid crystal layer was calibrated for color-temperature correspondence by using a thermocouple attached to each heated Inconel sheet. A dark blue color corresponded to the highest temperature, and blue, green, yellow, and reddish-brown corresponded to decreasing levels of temperature. The yellow color occurred over the narrowest temperature band of 0.06 °C and was, therefore, the color used for temperature measurement. Varying the electrical heat input to the sheet under flow conditions enabled the yellow color location to be changed. The liquid crystal was calibrated by positioning the yellow color at the same location as the thermocouple. The yellow color was calibrated at 37.8 °C.

Station number	Distance from beginning of test section, x (cm)
①	6.35
②	40.01
③	54.61
④	60.96
⑤	69.22
⑥	100.33

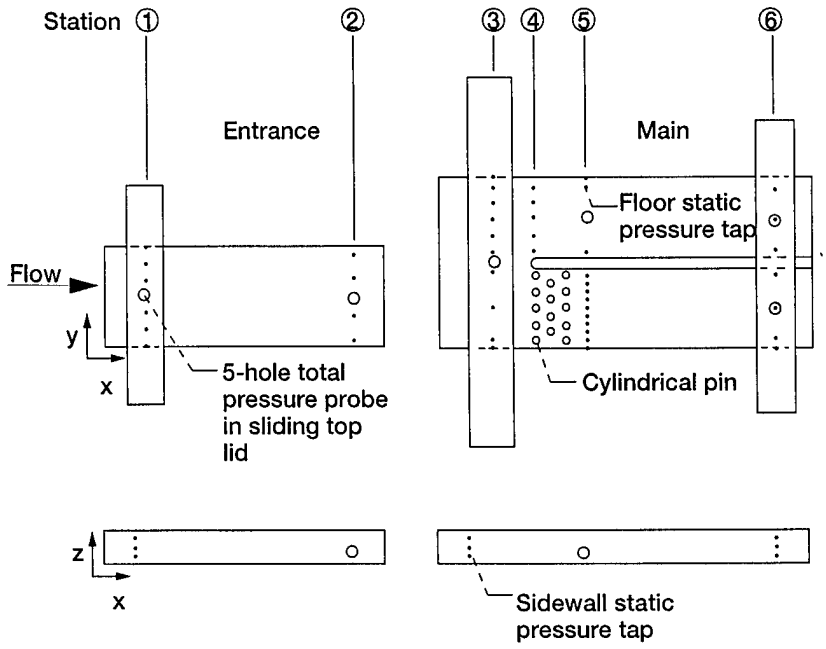

Figure 5.—Discrete hole pressure measurement locations.

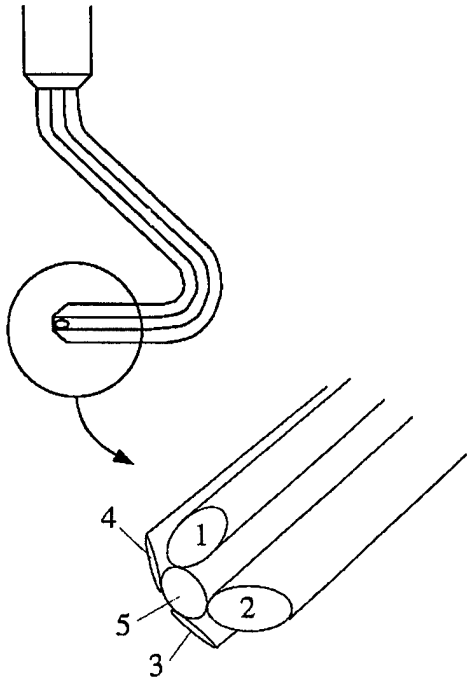

Figure 6.—Five-hole total pressure probe.

Experimental Measurements

Entrance Velocity Profile and Turbulence Intensity.—Velocity profiles were measured near the upstream end of the entrance test section (station 1) by using a surface static pressure tap and a vertically traversable boundary layer total pressure probe located near the horizontal center of the channel. The probe was moved in small increments from the floor surface to a location just above the midchannel height position. It was not possible to measure the profiles at higher positions because of restrictions imposed by the equipment. Since the entrance passage geometry was symmetrical about the midchannel height position, it was assumed that the velocity profile was symmetrical. Free-stream turbulence intensity was also measured at this location with hot-wire anemometry. All the measurements were made at nominal entrance Reynolds numbers of 45 000, 335 000, and 726 000, corresponding roughly to velocities of 9, 67, and 155 m/sec, respectively.

Heat Transfer.—Heat transfer tests were performed at three nominal entrance Reynolds numbers of Re = 45 000, 335 000, and 726 000. The operating procedure was initiated by bringing the tunnel to the velocity necessary to produce the desired Reynolds number. Electric power was then supplied to both entrance and main test section Inconel sheets at a matching heat flux (Q/A). This raised the temperature of the liquid crystal to the point at which color patterns appeared. The location of the yellow color lines was varied over the surface by changing the power input while the free-stream velocity remained the same. Sufficient time was given between data recordings to allow thermal equilibrium to occur. Typically about 15 min was allowed. Data were taken by four charged couple device (CCD) color video cameras mounted well above the test section. One camera viewed the entire entrance section, and another camera viewed the entire main test section. The other two cameras were positioned to give closeup views of the cylindrical pin area. The data were recorded on S-VHS video tape. A photograph of the test section under flow conditions is shown in figure 7. The color-temperature patterns on the surface can be clearly seen.

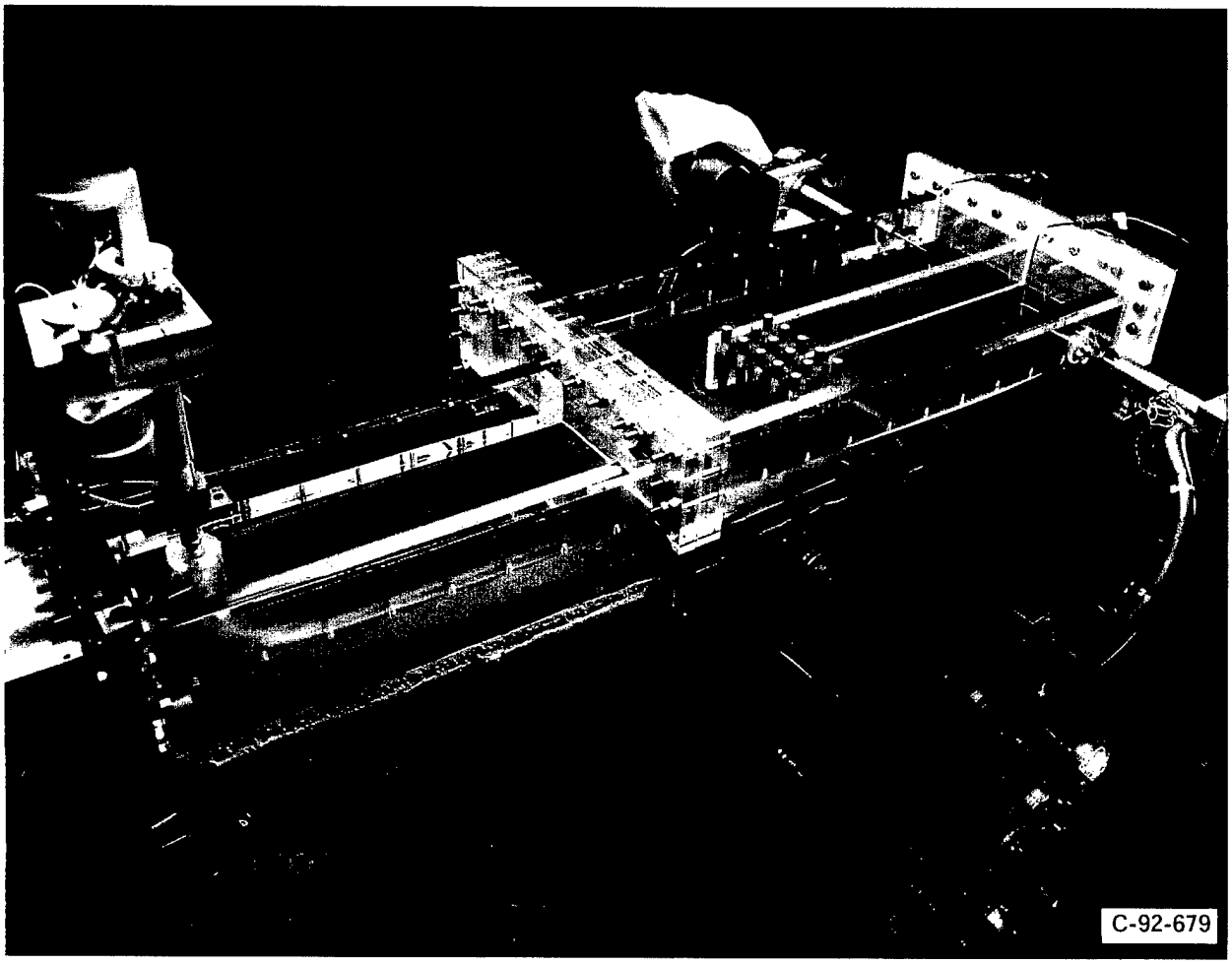

Figure 7.—Test section under flow conditions ($Re_{entrance}$ = 45 000).

Surface heat transfer coefficients were calculated as

$$h = \frac{(Q_e - Q_L)}{A(T_{LC} - T_R)}$$

The local heat transfer coefficient h was calculated at the location of the calibrated color band (an isotherm which in this case also represents a uniform heat transfer coefficient). The heat energy Q_e supplied to the heater sheet was calculated from the measured voltage across the sheet and the current through a shunt resistor in series with the sheet. The heat loss Q_L was the calculated radiation from the surface. The insulation under the test cell floor prevented backside heat loss. Other heat losses were estimated to be negligible. The area A was the measured area of the Inconel heater sheet. The temperature of the test surface T_{LC} was the calibrated liquid crystal temperature. The recovery temperature T_R of the entrance free-stream air was calculated as

$$T_R = T_s + r(T_t - T_s)$$

where T_s and T_t are the static and total air temperatures respectively, and r is the recovery factor, defined as $Pr^{1/3}$.

The heat transfer video data reduction was done with a personal computer equipped with a commercial video frame grabbing board. A computer program was written to manually digitize (trace) the yellow color bands from a video image grabbed from the video tape. The digitized locations along with the measurements of surface heat flux, air temperature, and free-stream velocity allowed the calculation of heat transfer coefficients.

Particle Flow Visualization.—Particle flow visualization tests were performed only at an entrance Reynolds number of 45 000. In these tests the flow was seeded with 1-μm polystyrene spheres which followed the flow field. These particles were suspended in a heated water-ethyl alcohol mixture and sprayed into the flow stream with a spray nozzle. By the time the mixture reached the test section, much of the liquid had evaporated. The particles were illuminated by a 7-W argon-ion laser. The laser beam, through a series of mirrors and lenses, was focused to a sheet of light approximately 2-mm thick. The result was a thin, illuminated, horizontal slice of the flow field

at midchannel height. A single black and white CCD video camera was used to record the flow onto S-VHS video tape. The trajectories of the particles were shown as streak lines on each video frame. In order to measure the velocity of the flow field, a light chopper was placed in the path of the laser beam. This chopper consisted of a rotating disk with holes spaced such that the light was periodically blocked. The maximum frequency of light chopping obtainable with this device was 3000 Hz. The instantaneous velocity of the particles was represented by the distance between interruptions in the streak lines on any one video frame as illustrated in figure 8. Similarly, the acceleration of the particles was represented by the change in the distance between interruptions in the streaks. Because of the high magnification required to see the particle traces, only one small area could be viewed at one time. A CAD software package was used to combine the data from approximately 300 individual frames so that all of the information could be presented in one composite picture.

The flow-field work is an extension of work done in conjunction with the University of Akron, where the procedure and the computerized data reduction method was initiated. Details of this method are given in reference 9. This present report includes enhanced data reduction and a much larger extension of the flow field such that it can be compared with the heat transfer results. The region of the test section that was mapped by using this technique was greatly increased to include an area from 8.9 cm upstream of the front row of pins to 3.8 cm downstream of the last row of pins.

Pressure Distribution Measurements.—Discrete, surface static pressure measurements were made at six different longitudinal stations as shown in figure 5. At three of these stations (1, 3, and 6 as indicated in fig. 5), five-hole total pressure probes were mounted on sliding lids, allowing full flow-field pressure measurements. Total pressure measurements were also made at stations 2 and 5 but only at midchannel height (horizontally) and in the center of the channel (vertically).

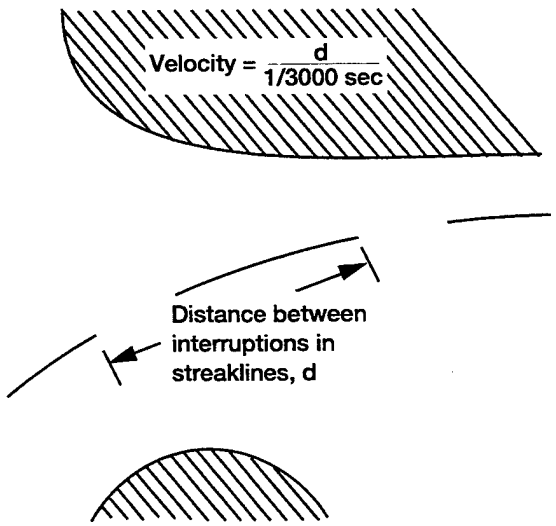

Figure 8.—Instantaneous velocity from 1/30-sec video frame, which uses 3000-Hz light chopper.

The automated electronic pressure recording system was calibrated immediately before each test and periodically throughout the test automatically. The system was programmed such that for each data location, 240 scans were recorded and averaged over 30 sec.

Pressure-Sensitive Paint.—In the pressure-sensitive paint method, the test surface was coated with a special paint which, after photo-excitation, emits light of varying intensity depending on the air pressure. The pressure-sensitive paint is an oxygen quenched, photoluminescent compound mixed with an oxygen permeable binder. The paint was excited with a filtered ultraviolet or blue light source that emits no light in the luminescence band. A very high resolution CCD black and white video camera viewed the model through a filter which removed all light except that which was emitted by the paint. The intensity of the emitted light is inversely proportional to the partial pressure of oxygen (and therefore air pressure). The distribution of pressure was computed from the distribution of light intensity (brighter points in image correspond to lower pressure). A video image processing system recorded the intensity in the images, and a personal-computer-based software program produced the static pressure maps. An explanation of the data reduction process is given in references 10 and 11.

Uncertainty Analysis

An uncertainty analysis was performed on the calculation of the experimental measurements based on the method described in references 12 and 13. The general results are shown in table II.

Included in the flow visualization and heat transfer uncertainties are errors largely dependent upon the accuracy of the operator during the digitizing process, for example reading the exact location of the isotherms. The high uncertainty for data at the low Reynolds number is due to the lower accuracy of

TABLE II.—UNCERTAINTY ANALYSIS RESULTS
[Reynolds number based on entrance hydraulic diameter.]

Experimental data (technique used to obtain)	Uncertainty, percent, based on Reynolds number (Re)—		
	45 000	335 000	726 000
Midchannel velocity vectors (flow visualization)	8	----	----
Surface heat transfer on channel floor (liquid crystal)	14	4	4
Cross-section velocity vectors at 5 axial stations (5-hole probe)	11	3	3
Surface static pressure (discrete pressure measurements)	0.13	0.17	0.30
Static pressures on channel floor (pressure-sensitive paint)	----	0.54	0.74
Entrance free-stream turbulence intensities (hot-wire anemometry)	16	3	2

measuring very small pressure differentials and low heat settings. The pressure measurement system had an accuracy of ±0.10 percent of the entire range of the transducers. The heater voltage and shunt measurements had fixed uncertainties of ±0.04 V and ±0.2 A, respectively.

Results And Discussion

Entrance Velocity Profiles and Turbulence Intensity

Velocity profiles at the entrance are shown in figure 9. As can be seen, fully developed channel flow had not occurred; as expected, there was a slight decrease in boundary layer thickness as velocity was increased. The boundary layer thickness, defined as the point where the velocity is 99 percent of the free-stream value, was 1.55 cm at Re = 45 000, 1.40 cm at Re = 335 000, and 0.94 cm at Re = 726 000.

The velocity profile data were also plotted logarithmically in terms of dimensionless coordinates and are shown in figure 10. This plot shows how the boundary layer compared with turbulent boundary layers normally encountered in turbine flow. Included in the figure is the calculated theoretical line for a fully turbulent boundary layer. The equations used were taken from reference 14. The experimental data matches the theoretical line fairly well.

The results of free-stream turbulence intensity measurements at midchannel height were 2.8 percent at a Reynolds number of 45 000, 1.2 percent at a Reynolds number of 335 000, and 2.9 percent at a Reynolds number of 726 000.

Heat Transfer Measurements

Quantitative heat transfer coefficients on the floor of the test section were mapped for the three different entrance Reynolds numbers. A typical example of the results is shown in figure 11. Figures 11(a) to (c) reproduce actual video screen photographs of the surface at the lowest Reynolds number of 45 000 and at three of the various electrical energy inputs. Also shown are closeup views of the color-temperature patterns around the pins. Figure 12(a) shows the corresponding map of heat transfer coefficients calculated from these isotherms, and figure 12(b) is a closeup of the area around the pins. Similar heat transfer maps are shown in figures 13 and 14 for Reynolds numbers of 335 000 and 726 000, respectively.

In general, the heat transfer patterns were similar for all Reynolds numbers. The heat transfer in the entrance region decreases going downstream. Areas of low heat transfer can be seen in the corner of the main test section where the flow is recirculating. The lowest values of heat transfer occurred in this region at all three flow conditions. In the unobstructed passage (no pins) there is a similarity in the pattern of the heat transfer at all three flow conditions with a high heat transfer coefficient coming off the partition leading edge, probably produced by the accelerating flow and high turbulence created in this area. Generally the value of heat transfer coefficients decreases as flow progresses downstream. Close to the partition, the coefficient values are smaller, probably because of a flow separation in this area. Looking at the closeup views of the pin region, the cooling effectiveness of the pins is evident by the color patterns immediately downstream of the pins and the corresponding

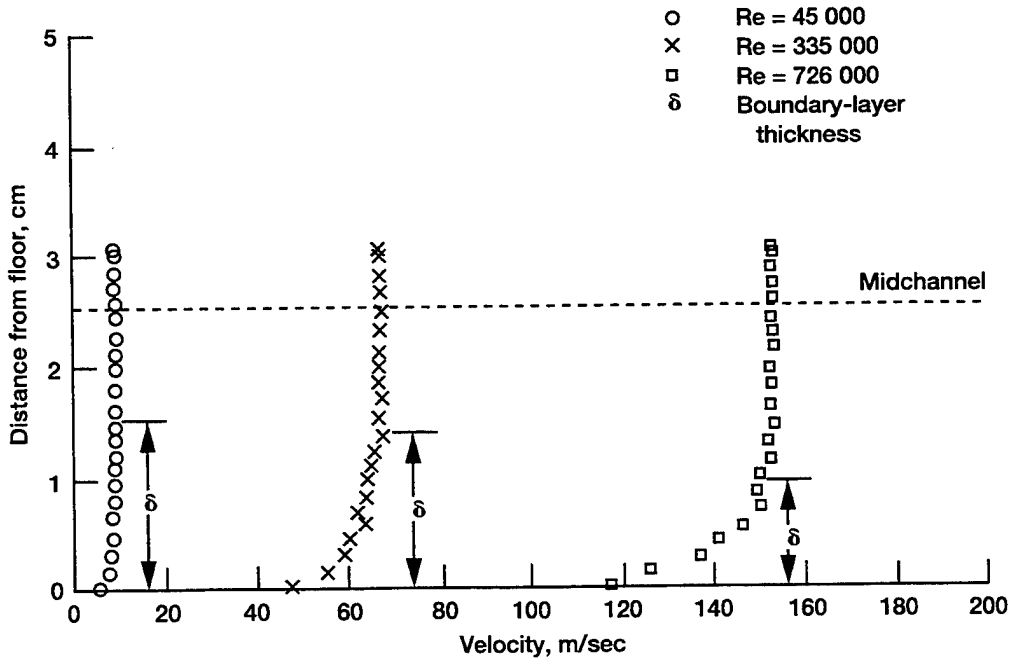

Figure 9.—Entrance velocity profiles.

high values of heat transfer coefficients. Further downstream of the pins, the heat transfer coefficients decrease. It should be noted that at some locations, the experimental contours were actually broadbands and not thin lines, indicating very gradual surface temperature gradients.

Particle Flow-Field Measurements

Particle image flow-field measurements were made at an entrance velocity of 9.14 m/sec, which corresponded to the lowest Reynolds number of 45 000. Attempts were made to obtain results at the higher Reynolds numbers, but these attempts were unsuccessful with the equipment which was available. As the velocity of the flow field was increased, it was more difficult to detect individual particle traces on the video screen. The maximum measurable particle velocity was further limited by the maximum frequency at which the light chopper could operate, which was 3000 Hz. As previously shown in figure 8, the velocity was determined by the distance between interruptions in the streaks shown in any one video frame. At higher velocities, streaks would appear in a single frame with either one interruption or no interruptions at all, making it impossible to determine the velocities or accelerations.

Figure 15(a) is a video picture of the particles as they flowed between a pin and the partition leading edge. Figure 15(b) shows the data after it was processed into velocity vectors. The magnitude of the velocity is indicated by the length of the arrows.

Figure 16 is a composite view of about 300 video frames giving an overall view of the flow field in the area investigated. Velocity vector diagrams similar to the one shown in figure 15(b) can be generated anywhere within this area from the data collected in this study. Figure 16 reveals a few features which help explain some of the heat transfer results. Immediately downstream of the pins, a turbulent area appears which corresponds to the high heat transfer area seen in the maps. In the unobstructed passage where the flow comes off the partition, there seems to be a region of turbulent flow bordered by an area of smooth accelerated flow. This corresponds to the high values of heat transfer seen on the heat transfer maps. In the recirculation corner of the main test section, the flow-mapping at first glance appears to indicate a highly turbulent, high-velocity area; however, actual observation of the flow showed this area to have very slow, three-dimensional flow, making it difficult to properly visualize the flow in a thin slice of light. This slow flow region would explain the low heat transfer and high surface temperatures indicated in the heat transfer tests. A comparison of the particle image velocity measurements with flow field velocities is made at the end of the next section.

Pressure Distribution Measurements

Figure 17 shows surface pressure measurements for the cross-section stations (looking upstream) indicated in figure 5 at the maximum Reynolds number of 726 000. As expected, the low surface pressure areas correspond with the high velocity areas. For example, the low pressure measurements shown in the right side of figure 17(b) at station 3 (~15 cm) reflect the accelerating flow approaching the open passage of the test section.

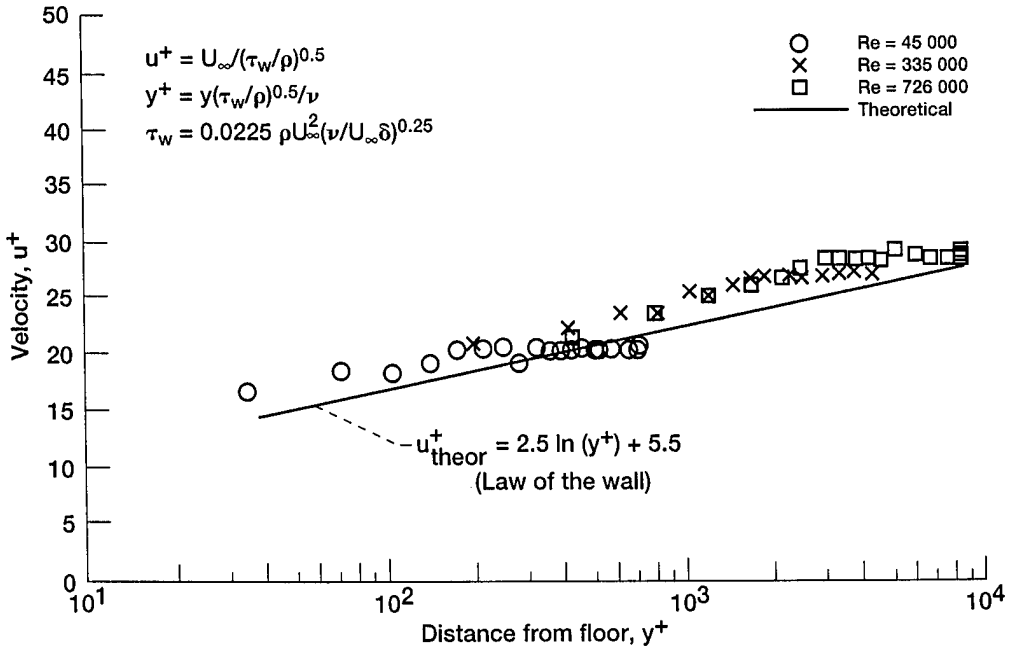

Figure 10.—Dimensionless boundary-layer profile.

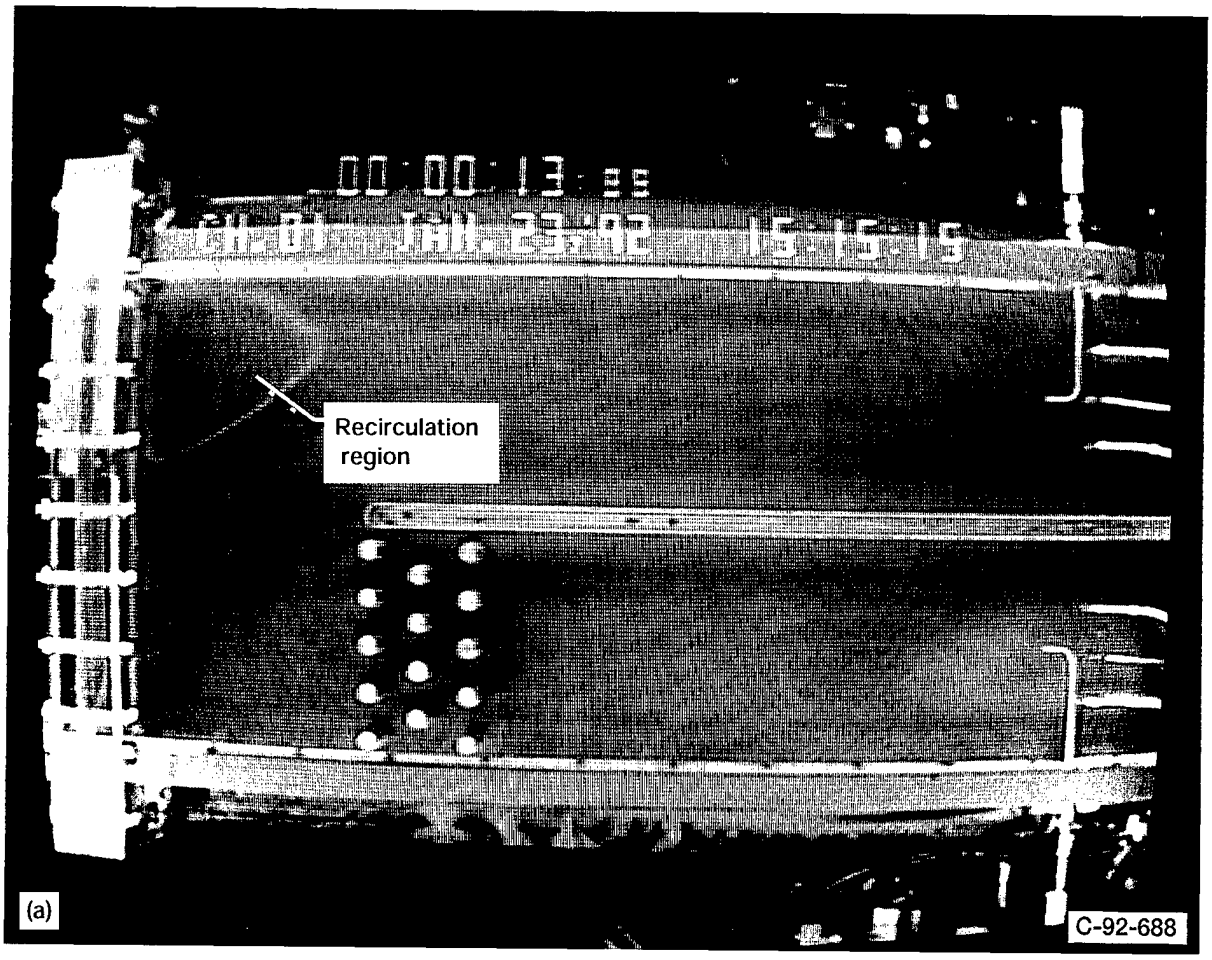

Figure 11.—Surface color-temperature patterns ($Re_{entrance}$ = 45 000). (a) Low heat input, main section. (b) Medium heat input. (c) High heat input.

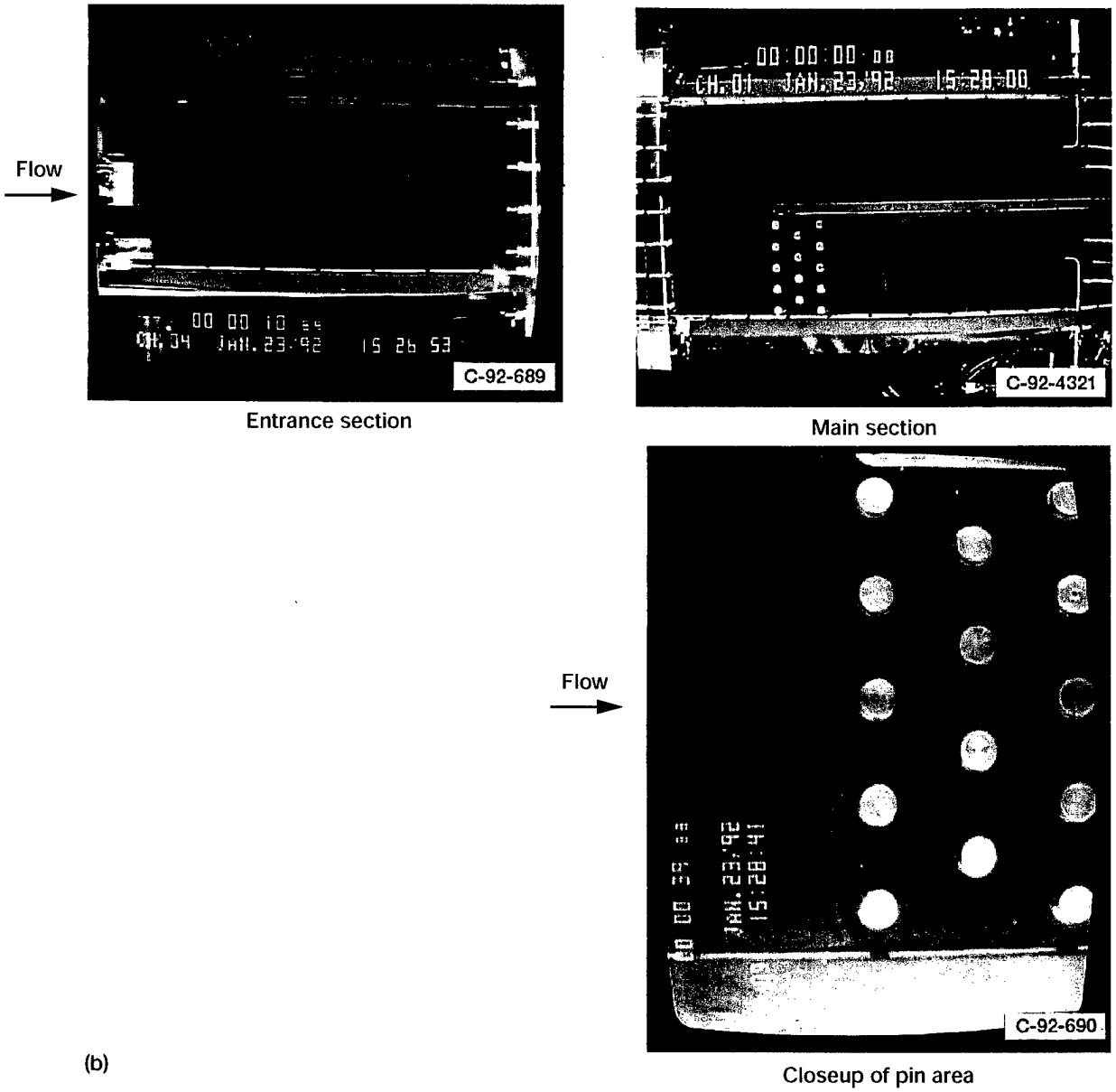

(b)

Figure 11.—Continued. (b) Medium heat input.

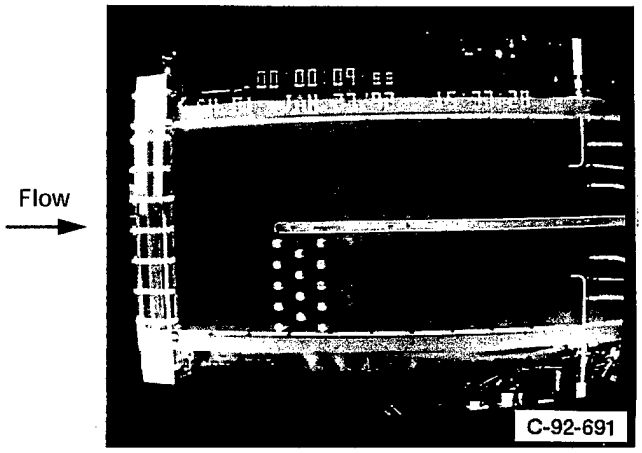

Main section

(c)

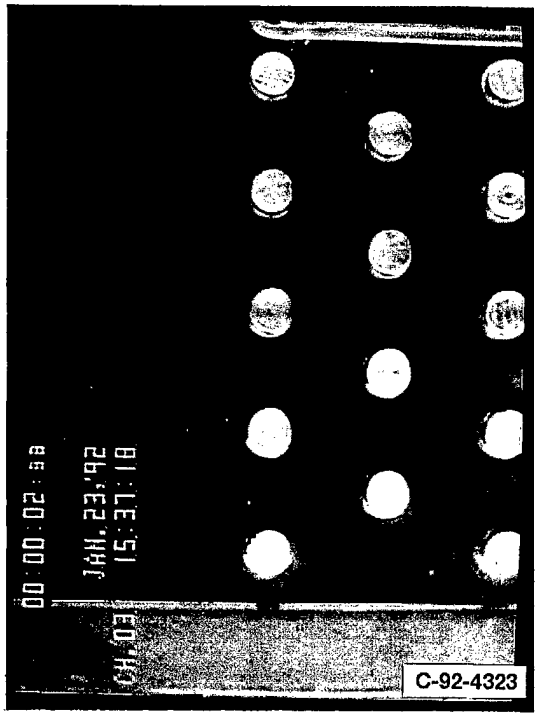

Closeup of pin array, upstream area

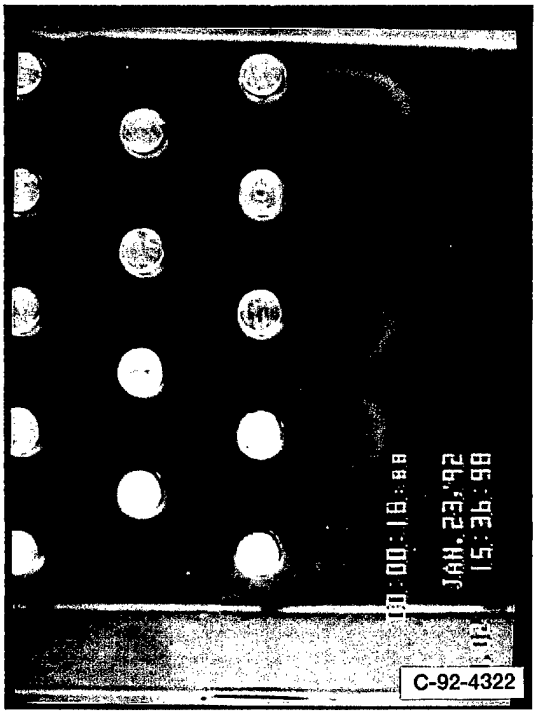

Closeup of pin array, downstream area

Figure 11.—Concluded. (c) High heat input.

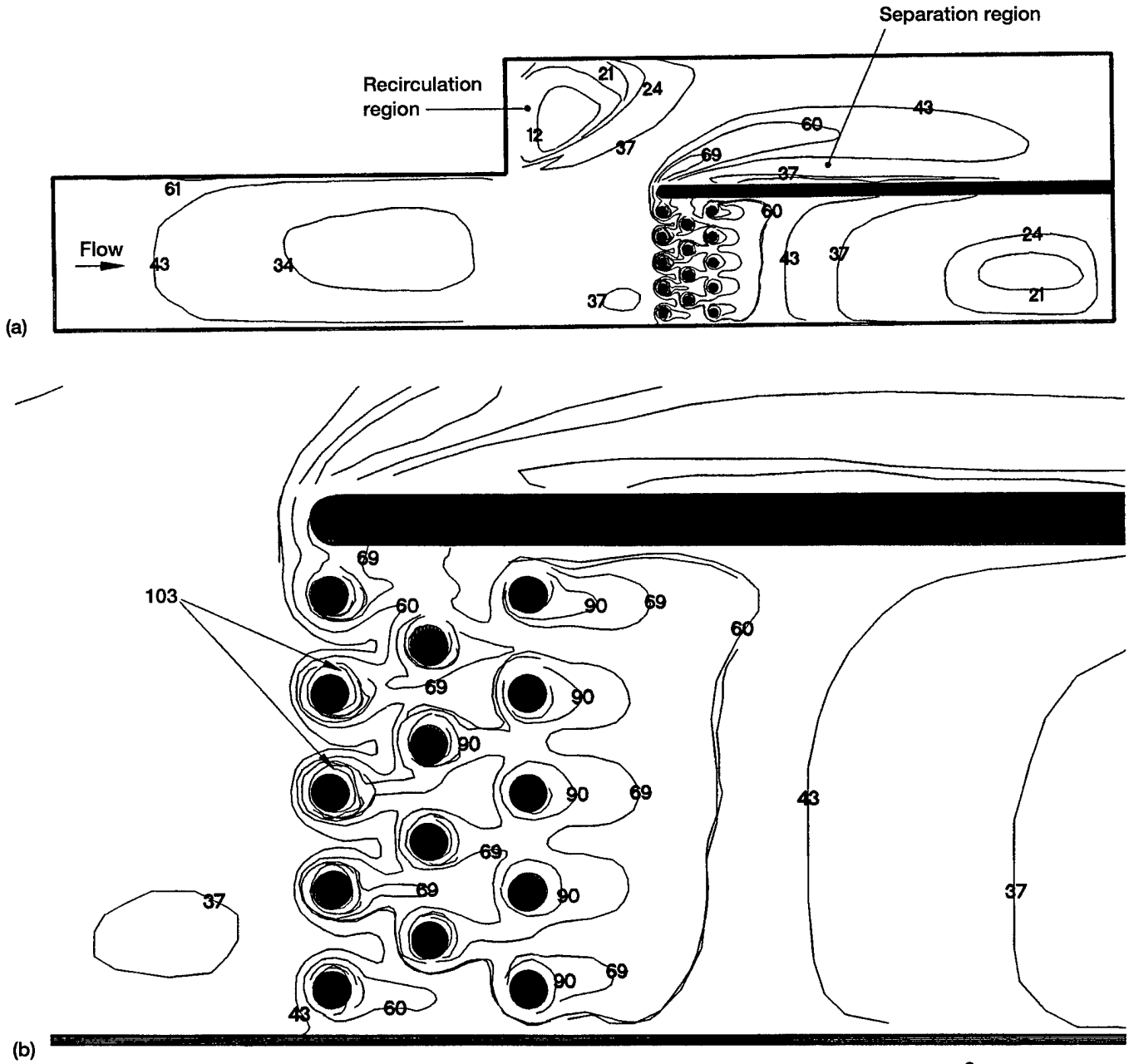

Figure 12.—Experimental heat transfer coefficients ($Re_{entrance}$ = 45 000). (Coefficients given in W/(m^2–K.) (a) Entire test section. (b) Closeup of pin area.

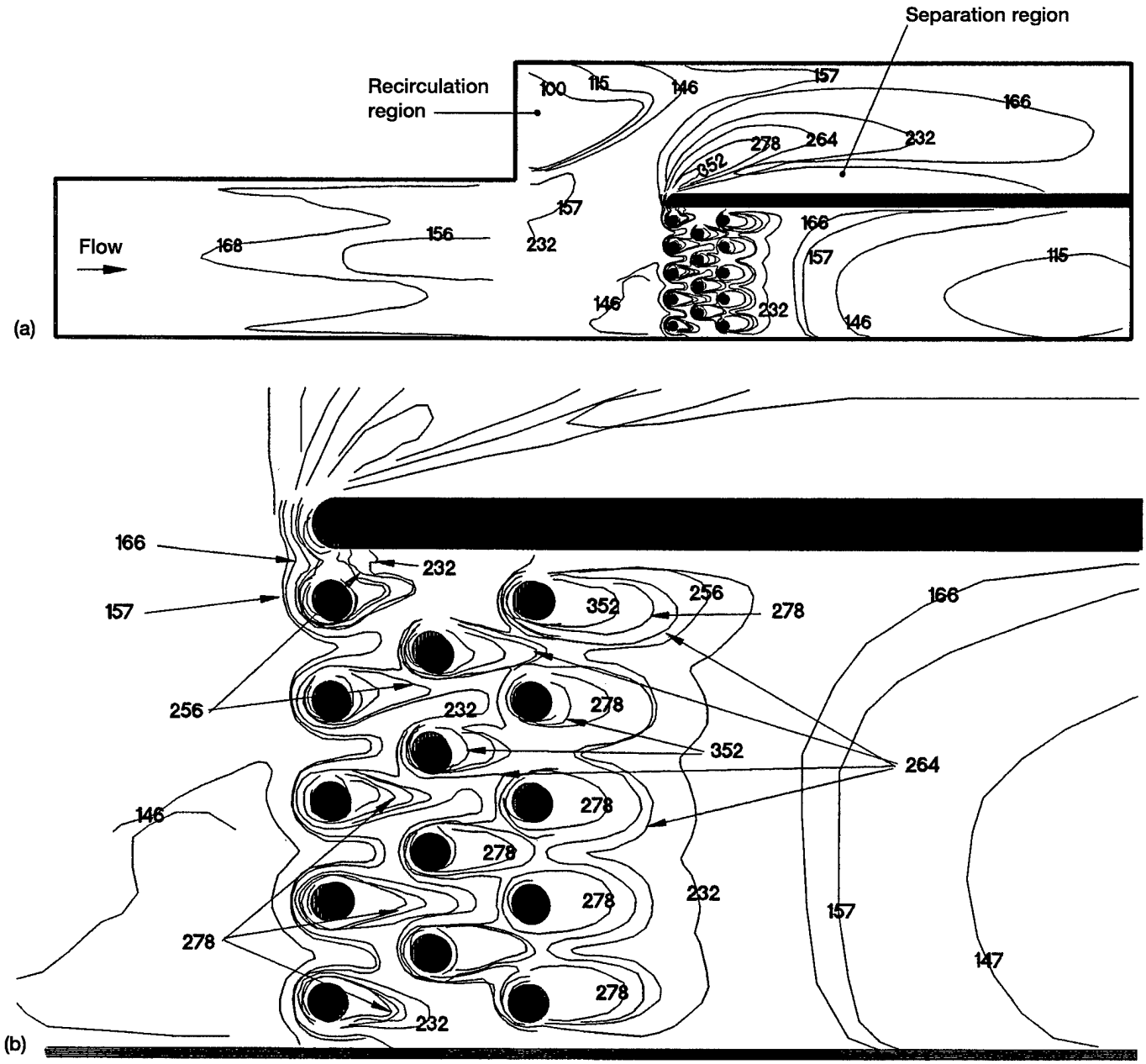

Figure 13.—Experimental heat transfer coefficients ($Re_{entrance}$ = 335 000). (Coefficients given in W/m2–K.) (a) Entire test surface. (b) Closeup of area.

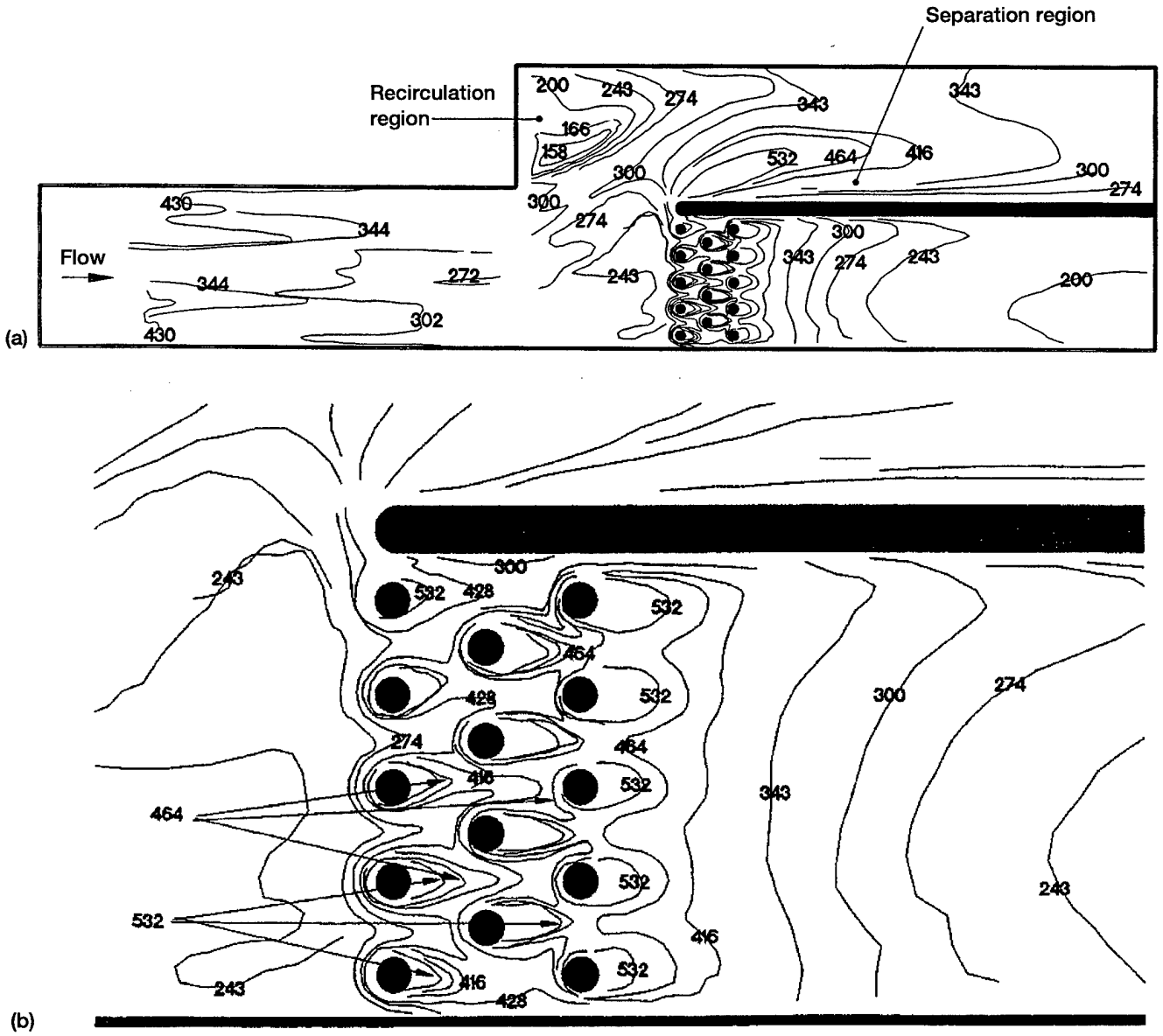

Figure 14.—Experimental heat transfer coefficients ($Re_{entrance}$ = 726 000). (Coefficients given in W/m2–K.) (a) Entire test surface. (b) Closeup of area.

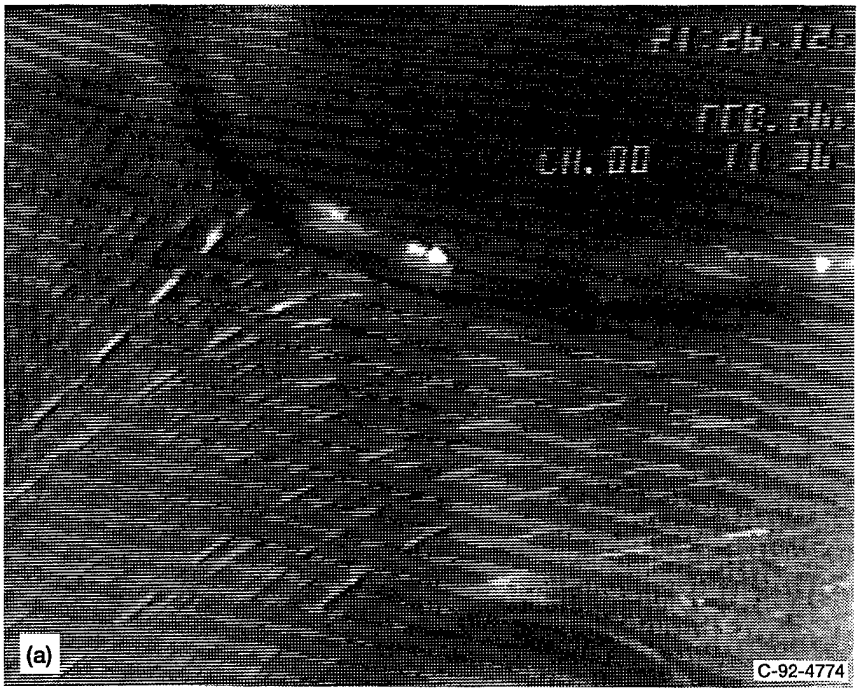

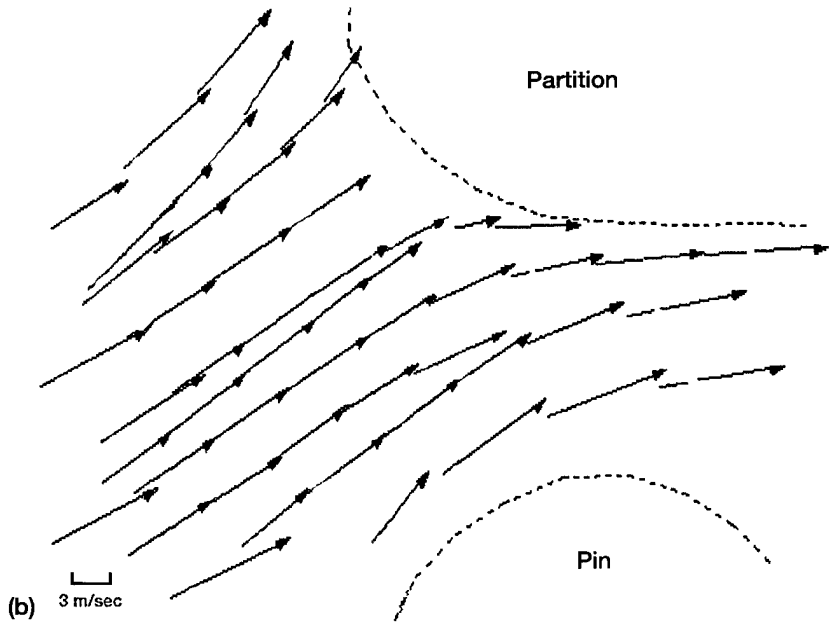

Figure 15.—Particle trajectories ($Re_{entrance}$ = 45 000). (a) Video picture. (b) Velocity vector diagram.

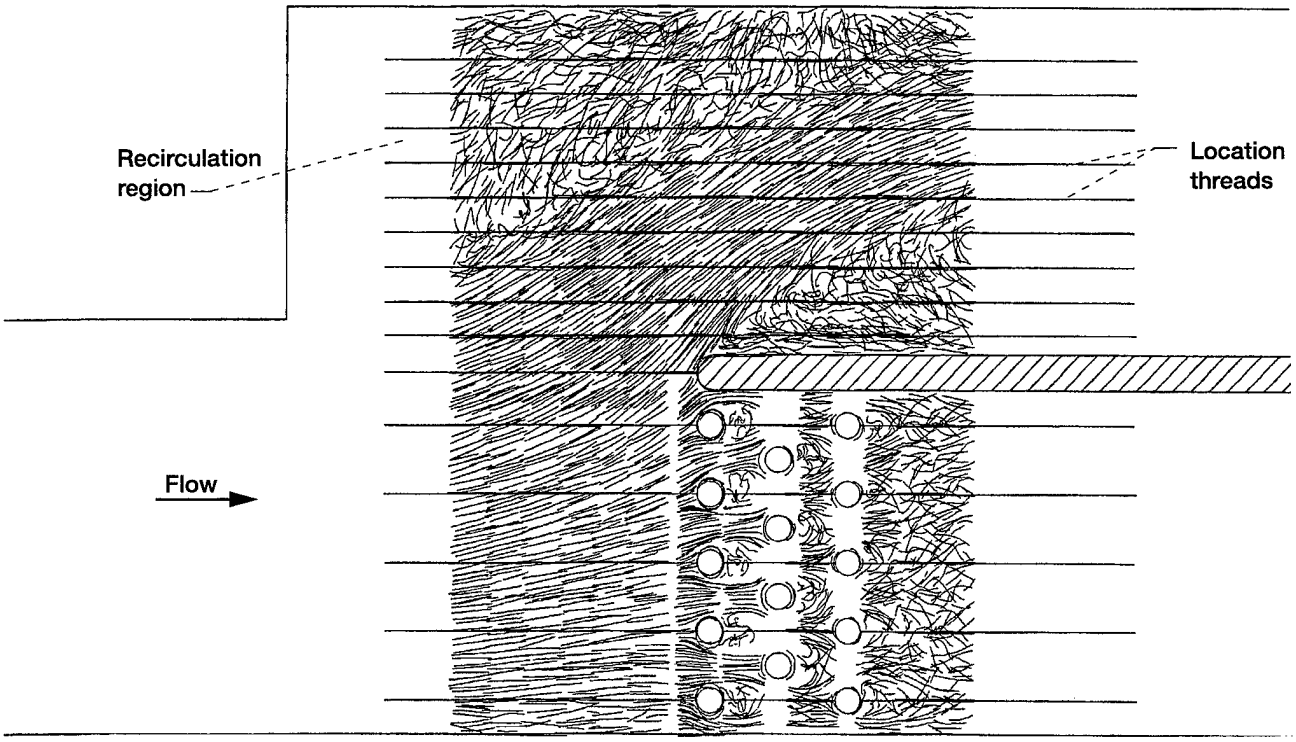

Figure 16.—Composite of digitized video data showing streamlines (300 video frames combined ($Re_{entrance}$ = 45 000).

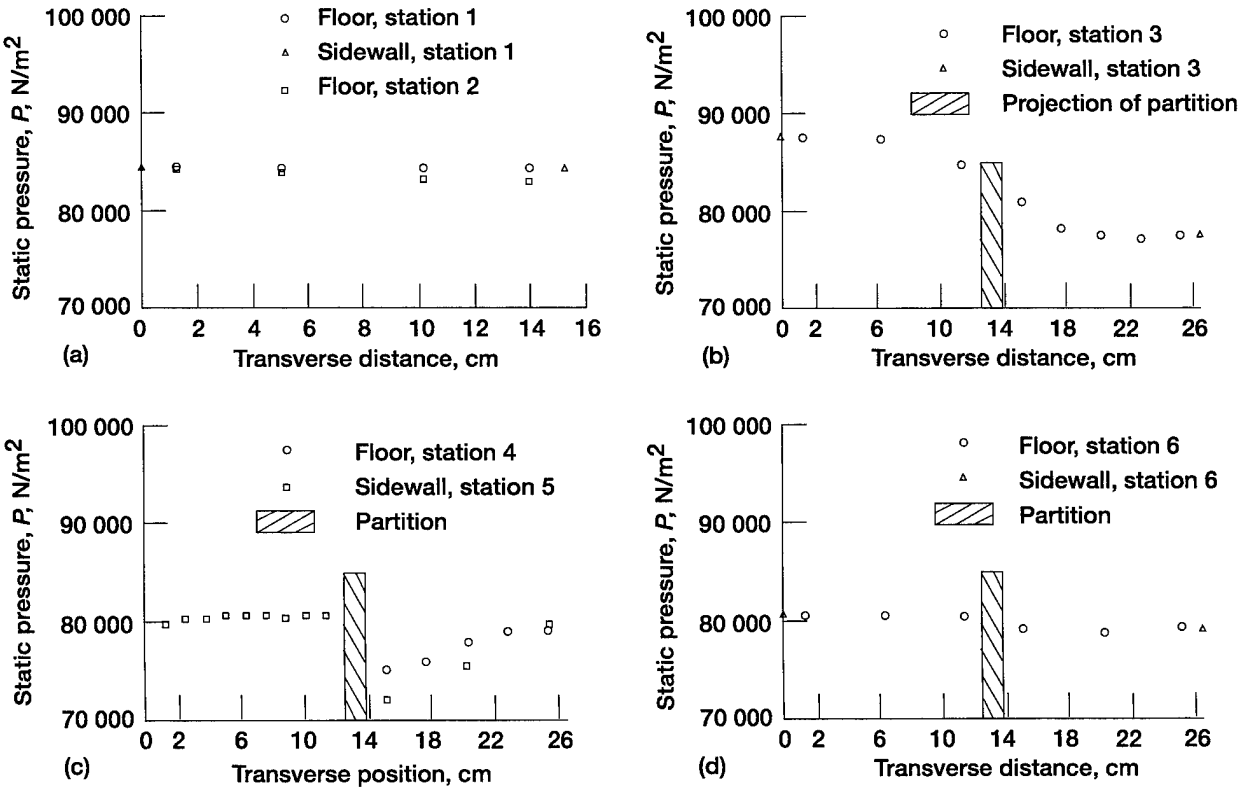

Figure 17.—Floor and sidewall static pressures (looking upstream). ($Re_{entrance}$ = 726 000).

The flow-field pressure measurements yielded quantitative velocity results. These results are shown in figure 18 for the maximum Reynolds number of 726 000 at the flow split area, station 3. Figure 18(a) is a map of the streamwise component u of velocity (in the direction of the tunnel) at station 3. The other two components of velocity, v and w (perpendicular to the tunnel direction) were also obtained. The resultants of these two components are shown in figure 18(b). The magnitude and direction of the resultants are indicated by the length and direction of the vectors shown in the figure. It can be seen that the highest velocities occurred in the accelerated flow region approaching the open passage area (~15 cm). The absence of flow-field data in the recirculation region (~18 cm) was due to the very small pressure differentials in this region.

Mass flow-rate splits in the main test section were also determined. Of the total mass flow, 55 percent passed through the unobstructed branch, and 45 percent passed through the pin-side branch. At the exit plane of the test section, the average total pressure was 96.7 kPa for the pin side and 96.6 kPa for the no-pins side at Re of 335 000; and 87.0 kPa for the pin side and 85.1 kPa for no-pins side at Re = 726 000.

In order to make a comparison between flow-field velocities measured by the total pressure probe and velocities measured by particle imaging, flow-field measurements were made at station 3 at midchannel height for an inlet Reynolds number of 45 000 at selected intervals across the channel. Velocities calculated from the probe data are shown in figure 19(a). Figure 19(b) shows velocities calculated from flow visualization at station 3 near the partition centerline. The velocities from these two methods compare reasonably well. Since flow visualization data could not be obtained at the higher flow rates, this is the only such comparison which could be made.

Pressure-Sensitive Paint Results

Figure 20 is a computer-generated map showing surface static pressures in the main test section, upstream (fig. 20(a)) and downstream (fig. 20(b)). The data shown were obtained at an entrance Re = 726 000. The color bars indicate the magnitude of the pressures. The map shows higher pressures upstream of the pins than downstream of the pins. It shows yet lower pressures in the unobstructed (no-pins) passage next to

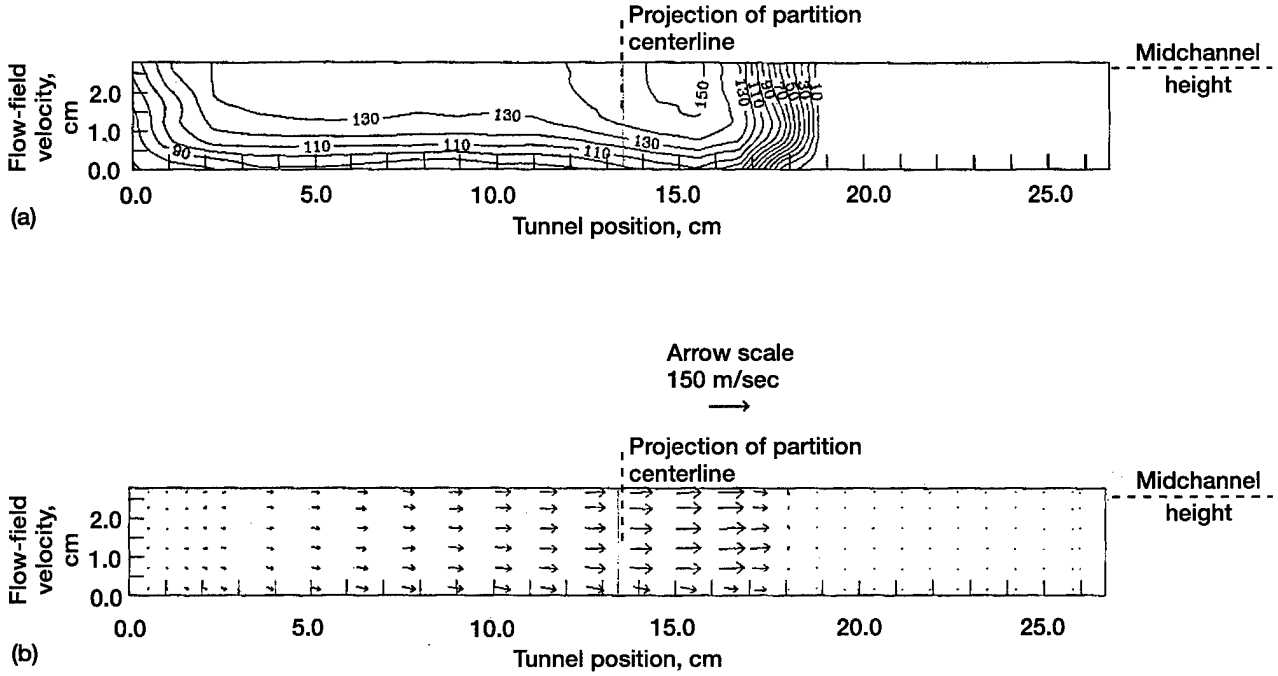

Figure 18.—Flow-field velocities at station 3 using total pressure probe (looking upstream; $Re_{entrance}$ = 726 000). (a) Velocity, u-component. (b) Velocity, v + w resultant.

the center partition where the velocity was shown to be high. In the downstream area of the unobstructed passage, the pressure is shown to increase as flow progressed. In the downstream area behind the pins, there is very little variation in the pressure.

The data yielded by the pressure sensitive paint (PSP) method showed good agreement with the data obtained at an entrance Reynolds number of 726 000 with the discrete hole method. This can be seen by comparing the results shown in figure 17 (discrete hole) with figure 20 (PSP). Figure 17(b) shows surface static pressures at station 3 in the flow split area. Floor static pressures are about 86 500 N/m^2 near the side wall on the pin side, decreasing slightly to 82 000 N/m^2 in front of the partition. This is also what figure 20 shows. On the unobstructed (no-pins) side, figure 17(b) shows the pressure decreasing from about 82 000 to about 77 000 N/m^2, again agreeing with figure 20. Comparisons made at other stations between figure 17 and the PSP data show similar favorable results.

The pressure sensitive paint method has the following advantages over the standard discrete hole method:

(1) It is completely nonintrusive.
(2) The data is obtained much more quickly.
(3) Measurements can be made at any desired location on the test surface instead of only where holes are located.

One disadvantage of the PSP method is the relative difficulty in obtaining data when extremely small pressure differentials are involved; however, the present study shows that pressure differential measurements as low as 345 N/m^2 (0.05 psi) are certainly possible.

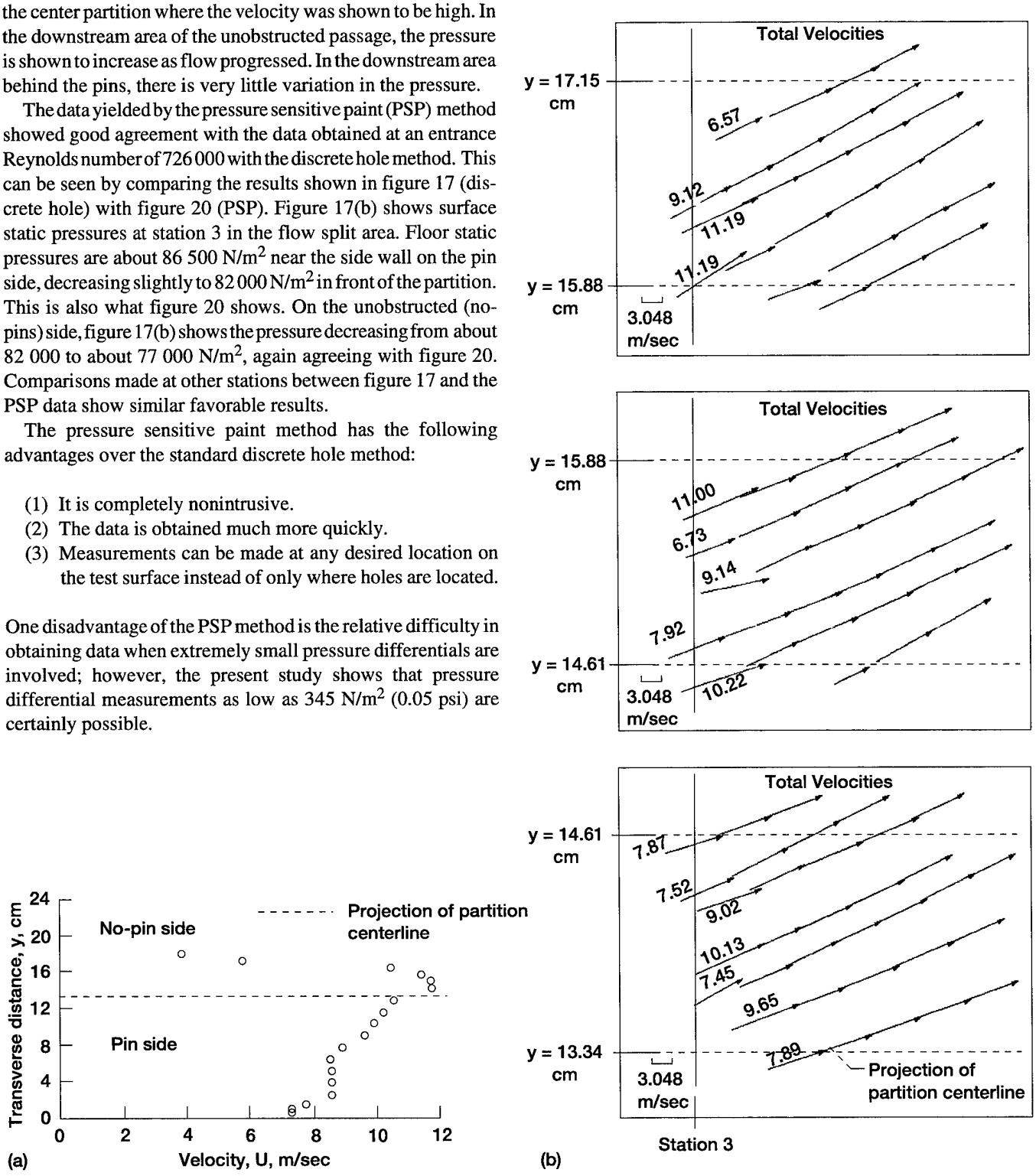

Figure 19.—Velocities at station 3 at midchannel height; ($Re_{entrance}$ = 45 000). (a) Flow-field velocities using total pressure probe. (b) Particle imaging velocity vectors.

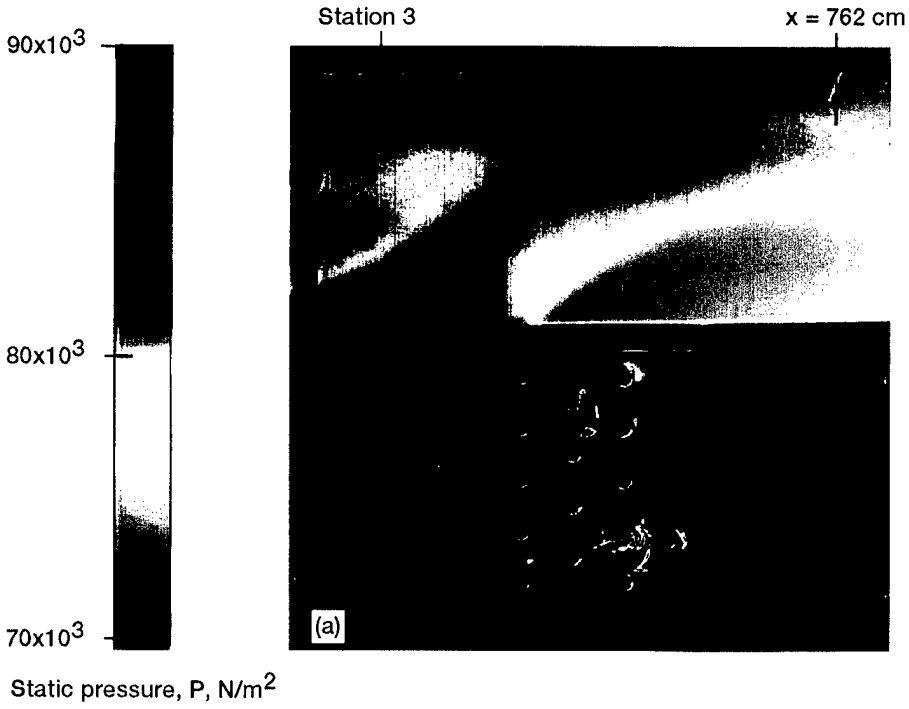

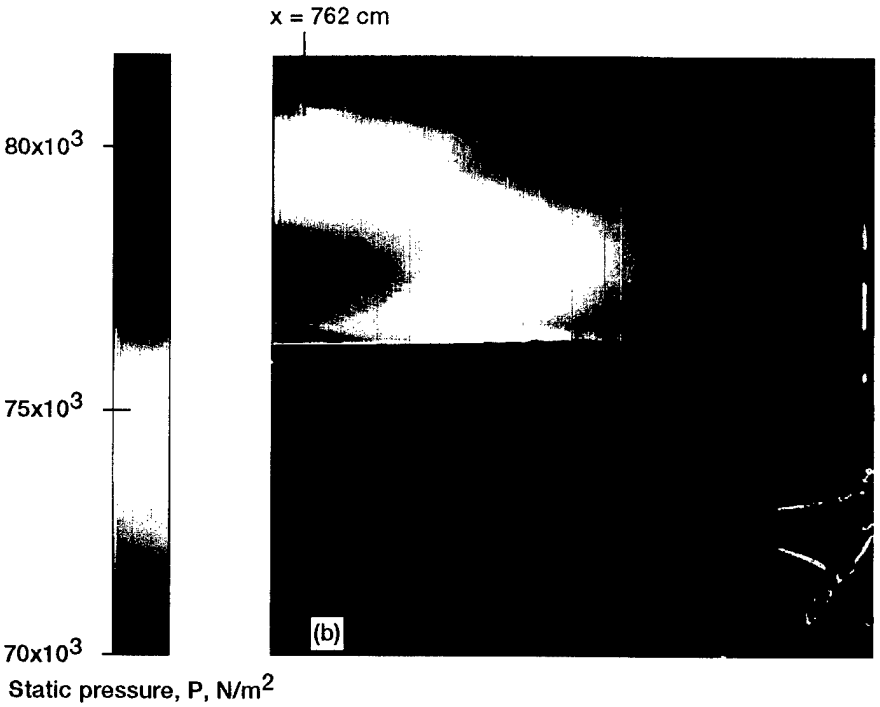

Figure 20.—Experimental floor static pressure maps from pressure sensitive paint technique ($Re_{entrance}$ = 726 000). (a) Flow split region. (b) Downstream end of test section.

Concluding Remarks

The experimental investigation revealed the physical conditions which exist during flow through a test section having some of the significant features of an internal passage of a cooled turbine blade. Three benchmark sets of data were produced, which are now available for internal cooling code validation: heat transfer, flow field, and pressure distribution. Areas of high and low heat transfer were identified, and quantitative heat transfer data were obtained over a range of flow conditions. The cooling effectiveness of the cylindrical pins was demonstrated. Areas of recirculating and separating flows and their effect on surface temperature patterns were evident. The experimental flow visualization data generally supported the heat transfer data in terms of explaining some of the temperature patterns. Surface pressure results obtained by using the relatively new pressure sensitive paint (PSP) method compared well with the results obtained with the more conventional discrete hole method of measuring surface pressure. The PSP method proved very promising for future use in measuring surface pressures.

National Aeronautics and Space Administration
Lewis Research Center
Cleveland, Ohio 44135, August, 1996

References

1. Becker, W.J.; and Steiner, A.L.: The Application of 3D Navier-Stokes Codes to Turbine Internal Cooling Problems. AIAA Paper 90–2267, July 1990.
2. Shih, T.I.-P.; Roelke, R.J.; and Steinthorsson, E.: Computations of the Three-Dimensional Flow and Heat Transfer Within a Coolant Passage of a Radial Turbine Blade. AIAA Paper 91–2238, June 1991.
3. Simoneau, R.J.; and Simon, F.: Progress Towards Understanding and Predicting Convection Heat Transfer in the Turbine Gas Path. NASA TM–105674, 1992.
4. Prakash, C.; and Zerkle, R.: Prediction of Turbulent Flow and Heat Transfer in a Radially Rotating Square Duct. J. Turbomach. vol. 114, Oct. 1992, pp. 835–846.
5. Snyder, P.H.; and Roelke, R.J.: Design of an Air-Cooled Metallic High-Temperature Radial Turbine. AIAA Paper 88–2872, July 1988.
6. Russell, L.M., et al.: Measurements and Computational Analysis of Heat Transfer and Flow in a Simulated Turbine Blade Internal Cooling Passage. AIAA Paper 93–1797, (NASA TM–106189), 1993.
7. Reichert, B.A.; and Wendt, B.J.: A New Algorithm for Five-Hole Probe Calibration, Data Reduction, and Uncertainty Analysis. NASA TM–106458, 1994.
8. Yavuzkurt, S.; A Guide to Uncertainty Analysis of Hot-Wire Data. J. Fluids Eng., vol. 106, June 1984, pp. 181–186
9. Braun M.J.; Canacci, V.A.; and Russell, L.M.: Full Field Flow Visualization and Computer-Aided Velocity Measurements in a Bank of Cylinders in a Wind Tunnel. Exp. Fluids, vol. 13, nos. 2–3, 1992, pp. 117–127.
10. Crites, R.C.: Pressure Sensitive Paint Technique. Meas. Tech Von Karman Institute Lecture Series, VKI-LS-1993-05, April 1993.
11. Bencic, T. J.: Experiences Using Pressure Sensitive Paint in NASA Lewis Research Center Propulsion Test Facilities. AIAA Paper 95–2831, 1995.
12. Abernethy, R.B.; and Benedict, R.P.: Measurement Uncertainty—A Standard Methodology. Proceedings of the 30th International Instrumentation Symposium (A85-46601 22-35), 1984. pp. 411–420.
13. Kline, S.J.; and McClintock, F.A.: Describing Uncertainties in Single-Sample Experiments. Mech. Eng., vol. 75, no.1, Jan. 1953, pp. 3–8.
14. Kays, W.M.: Convective Heat and Mass Transfer. McGraw-Hill, New York, 1966.

REPORT DOCUMENTATION PAGE

Form Approved
OMB No. 0704-0188

1. AGENCY USE ONLY (*Leave blank*)	2. REPORT DATE	3. REPORT TYPE AND DATES COVERED
	December 1997	Technical Paper

4. TITLE AND SUBTITLE

Measurements of Heat Transfer, Flow, and Pressures in a Simulated Turbine Blade Internal Cooling Passage

5. FUNDING NUMBERS

WU–505–62–52
1L161102AH45

6. AUTHOR(S)

Louis M. Russell, Douglas R. Thurman, Philip E. Poinsatte, and Steven A. Hippensteele

7. PERFORMING ORGANIZATION NAME(S) AND ADDRESS(ES)

NASA Lewis Research Center
Cleveland, Ohio 44135–3191
and
U.S. Army Research Laboratory
Cleveland, Ohio 44135–3191

8. PERFORMING ORGANIZATION REPORT NUMBER

E–10404

9. SPONSORING/MONITORING AGENCY NAME(S) AND ADDRESS(ES)

National Aeronautics and Space Administration
Washington, DC 20546–0001
and
U.S. Army Research Laboratory
Adelphi, Maryland 20783–1145

10. SPONSORING/MONITORING AGENCY REPORT NUMBER

NASA TP–3646
ARL–TR–923

11. SUPPLEMENTARY NOTES

Louis M. Russell, Philip E. Poinsatte, and Steven A. Hippensteele, NASA Lewis Research Center; Douglas R. Thurman, Vehicle Propulsion Directorate, U.S. Army Research Laboratory, Lewis Research Center. Responsible person, Douglas R. Thurman, organization code 0300, (216) 433–6573.

12a. DISTRIBUTION/AVAILABILITY STATEMENT

Unclassified - Unlimited
Subject Category: 34 Distribution: Standard

This publication is available from the NASA Center for AeroSpace Information, (301) 621–0390.

12b. DISTRIBUTION CODE

13. ABSTRACT ***(Maximum 200 words)***

An experimental study was made to obtain quantitative information on heat transfer, flow, and pressure distribution in a branched duct test section that had several significant features of an internal cooling passage of a turbine blade. The objective of this study was to generate a set of experimental data that could be used for validation of computer codes that would be used to model internal cooling. Surface heat transfer coefficients and entrance flow conditions were measured at nominal entrance Reynolds numbers of 45 000, 335 000, and 726 000. Heat transfer data were obtained by using a steady-state technique in which an Inconel heater sheet is attached to the surface and coated with liquid crystals. Visual and quantitative flow-field data from particle image velocimetry measurements for a plane at midchannel height for a Reynolds number of 45 000 were also obtained. The flow was seeded with polystyrene particles and illuminated by a laser light sheet. Pressure distribution measurements were made both on the surface with discrete holes and in the flow field with a total pressure probe. The flow-field measurements yielded flow-field velocities at selected locations. A relatively new method, pressure sensitive paint, was also used to measure surface pressure distribution. The pressure paint data obtained at Reynolds numbers of 335 000 and 726 000 compared well with the more standard method of measuring pressures by using discrete holes.

14. SUBJECT TERMS	15. NUMBER OF PAGES
Heat transfer; Flow visualization; Liquid crystals; Internal cooling; Particle image; Velocimetry; Pressure sensitive paint	29
	16. PRICE CODE A03

17. SECURITY CLASSIFICATION OF REPORT	18. SECURITY CLASSIFICATION OF THIS PAGE	19. SECURITY CLASSIFICATION OF ABSTRACT	20. LIMITATION OF ABSTRACT
Unclassified	Unclassified	Unclassified	